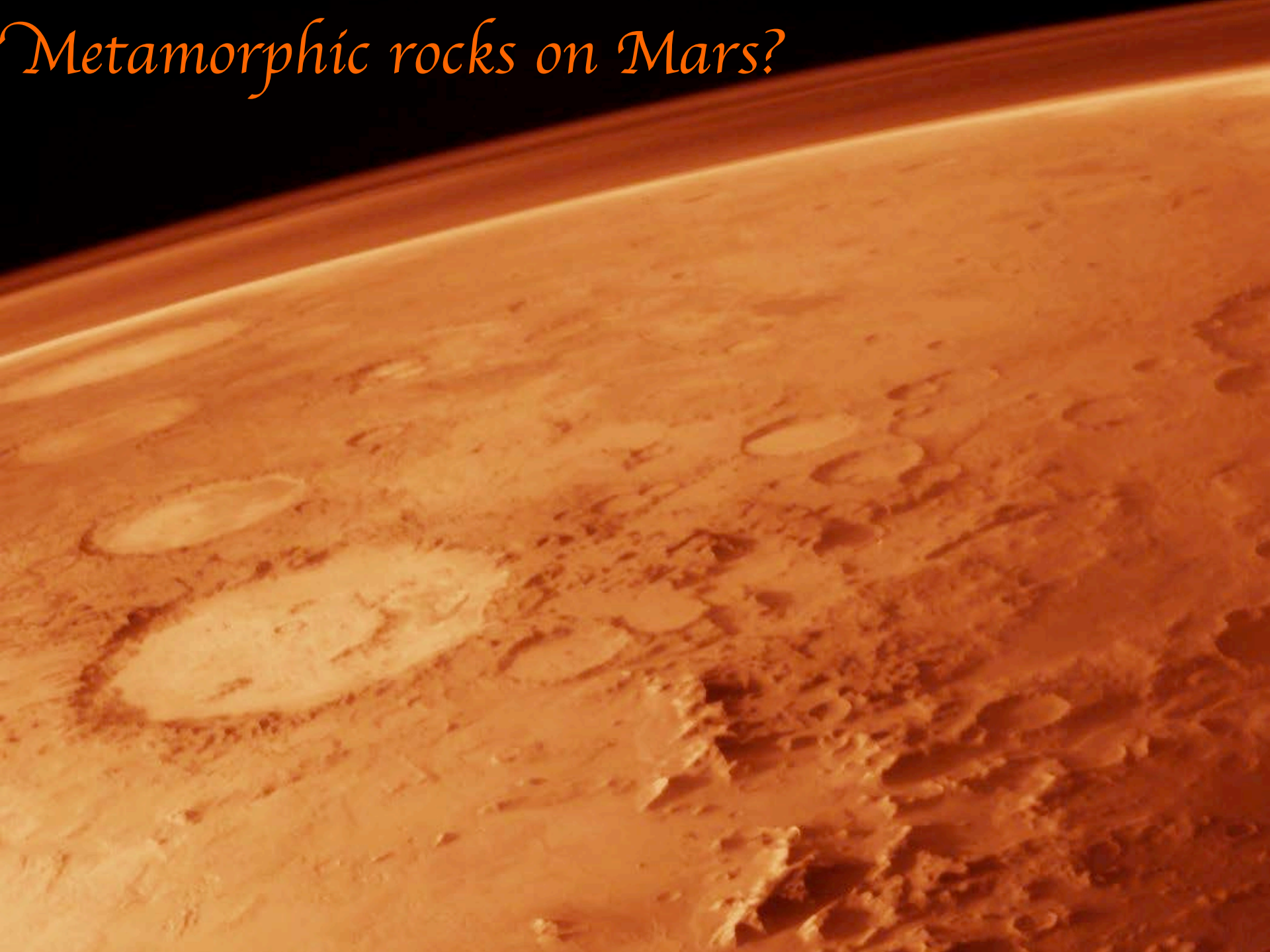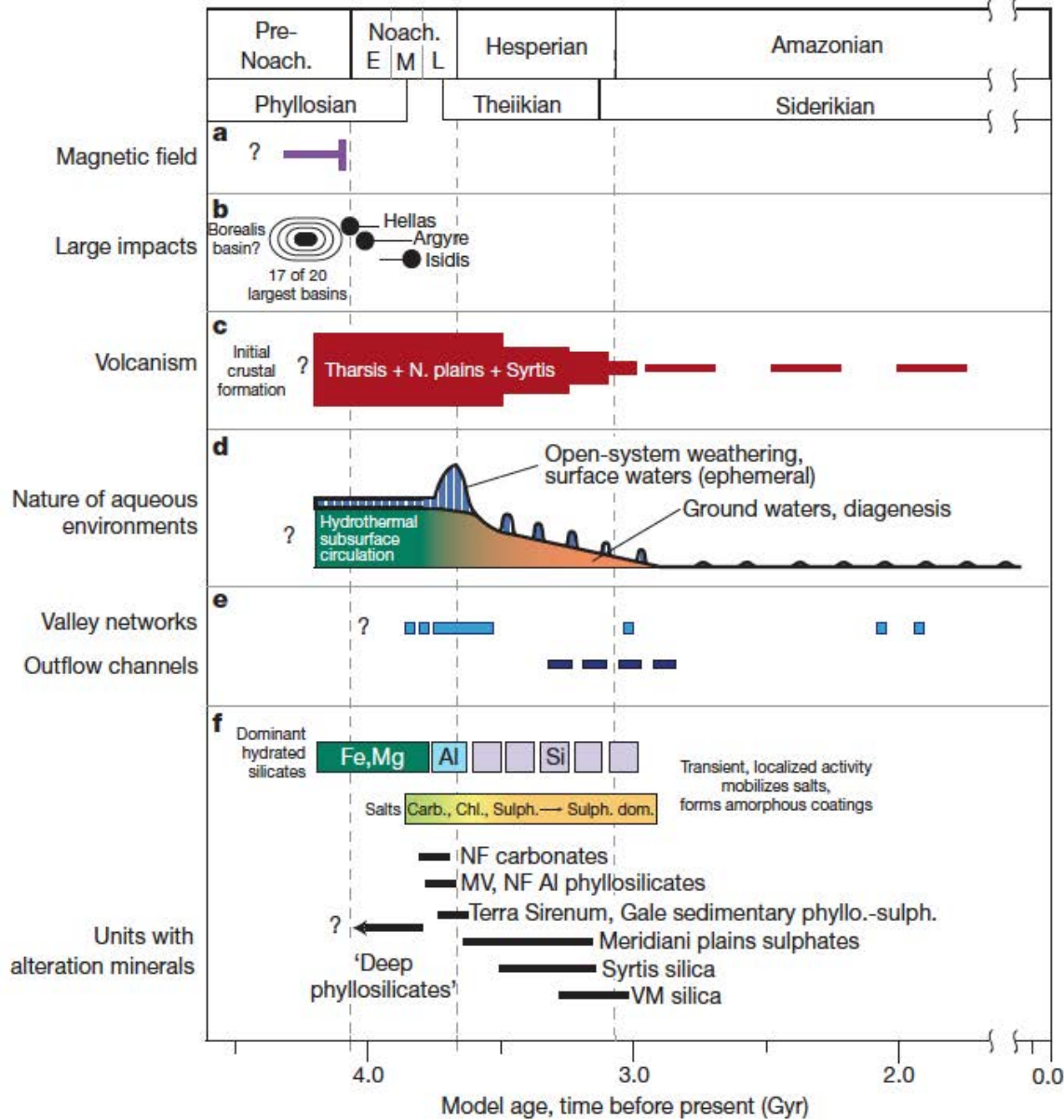# Metamorphic rocks on Mars?
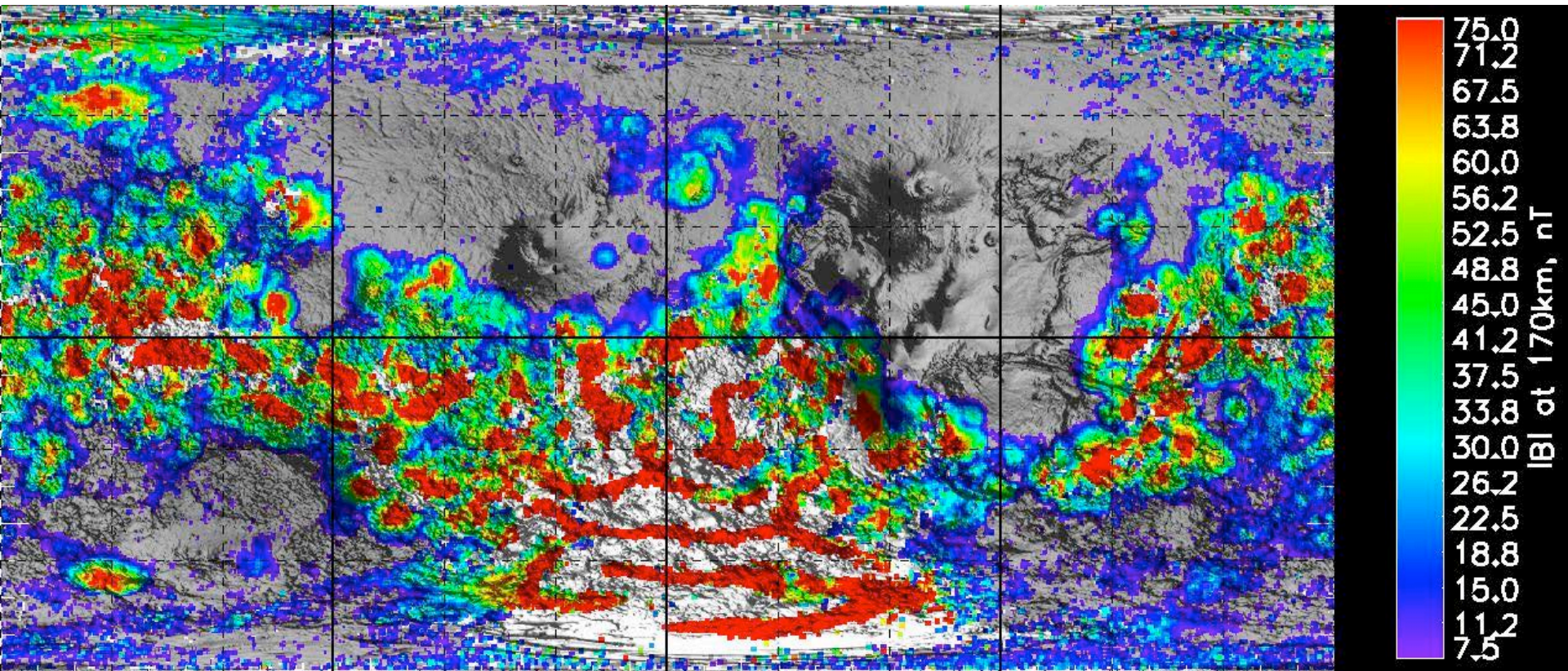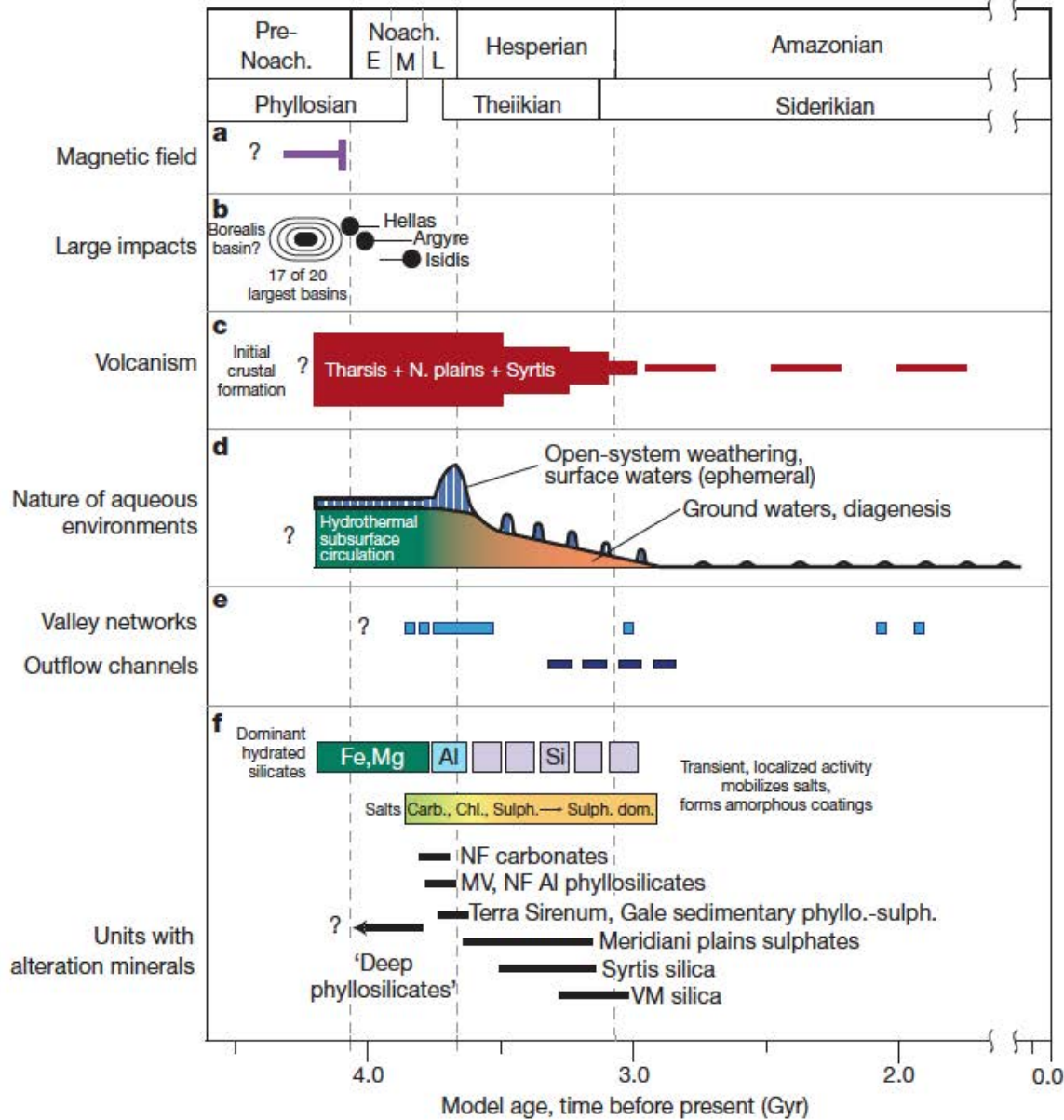
Ehlmann et al. (2011a)

Figure 4 | Timeline of major processes in Mars history. a–c, Major geological processes influencing water availability, including the presence of a magnetic field[95] (a), impact cratering[96,97] (b) and volcanism[86,98] (c). **d,** Schematic depicting the changing nature of environments hosting liquid water, as implied by the geological evidence discussed herein. **e, f,** Evidence of liquid water: timing of valley network and outflow channel activity[15,16] ages of key minerals formed by aqueous alteration (e) and important regional units with alteration minerals (f). Relative timing is determined using relative crater densities and stratigraphic relationships. Absolute ages of period boundaries[5] have uncertainties of several hundred million years, inherent to extrapolation from cratering statistics[99]. NF, Nili Fossae; MV, Mawrth Vallis; VM, Valles Marineris; Carb., carbonates; Chl., chlorites; Sulph., sulphates.
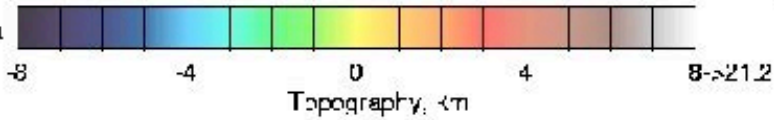
Mars magnetic field

Ehlmann et al. (2011a)

Figure 4 | Timeline of major processes in Mars history. a–c, Major geological processes influencing water availability, including the presence of a magnetic field[95] (a), impact cratering[96,97] (b) and volcanism[86,98] (c). **d,** Schematic depicting the changing nature of environments hosting liquid water, as implied by the geological evidence discussed herein. **e, f,** Evidence of liquid water: timing of valley network and outflow ch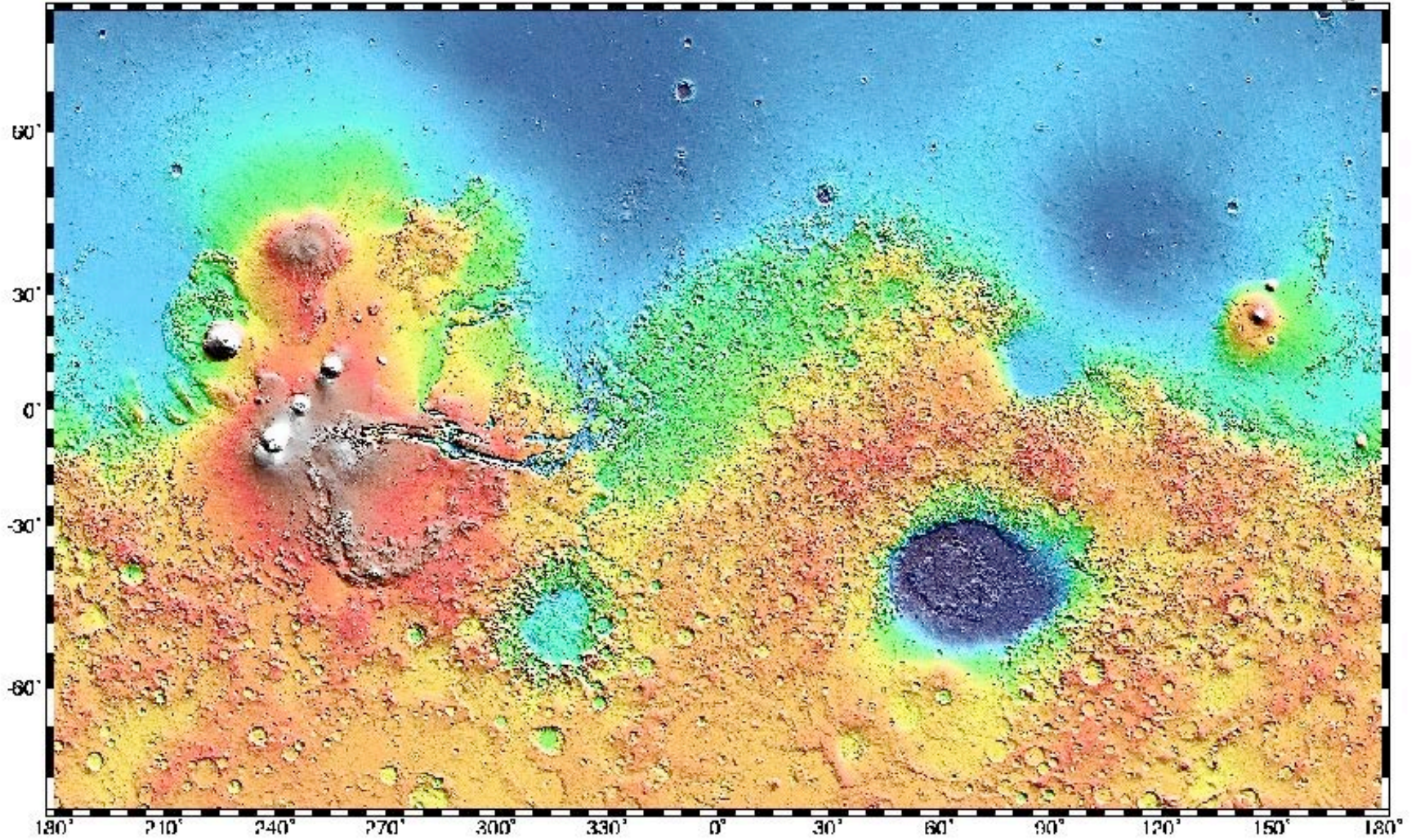annel activity[15,16] ages of key minerals formed by aqueous alteration (e) and important regional units with alteration minerals (f). Relative timing is determined using relative crater densities and stratigraphic relationships. Absolute ages of period boundaries[5] have uncertainties of several hundred million years, inherent to extrapolation from cratering statistics[99]. NF, Nili Fossae; MV, Mawrth Vallis; VM, Valles Marineris; Carb., carbonates; Chl., chlorites; Sulph., sulphates.

MOLA Science Team

Topography, km

-8   -4   0   4   8->21.2

NASA-Goddard
Space Flight Center

NASA

Ehlmann et al. (2011a)

Figure 4 | Timeline of major processes in Mars history. a–c, Major geological processes influencing water availability, including the presence of a magnetic field[95] (a), impact cratering[96,97] (b) and volcanism[86,98] (c). **d,** Schematic depicting the changing nature of environments hosting liquid water, as implied by the geological evidence discussed herein. **e, f,** Evidence of liquid water: timing of valley network and outflow channel activity[15,16] ages of key minerals formed by aqueous alteration (e) and important regional units with alteration minerals (f). Relative timing is determined using relative crater densities and stratigraphic relationships. Absolute ages of period boundaries[5] have uncertainties of several hundred million years, inherent to extrapolation from cratering statistics[99]. NF, Nili Fossae; MV, Mawrth Vallis; VM, Valles Marineris; Carb., carbonates; Chl., chlorites; Sulph., sulphates.
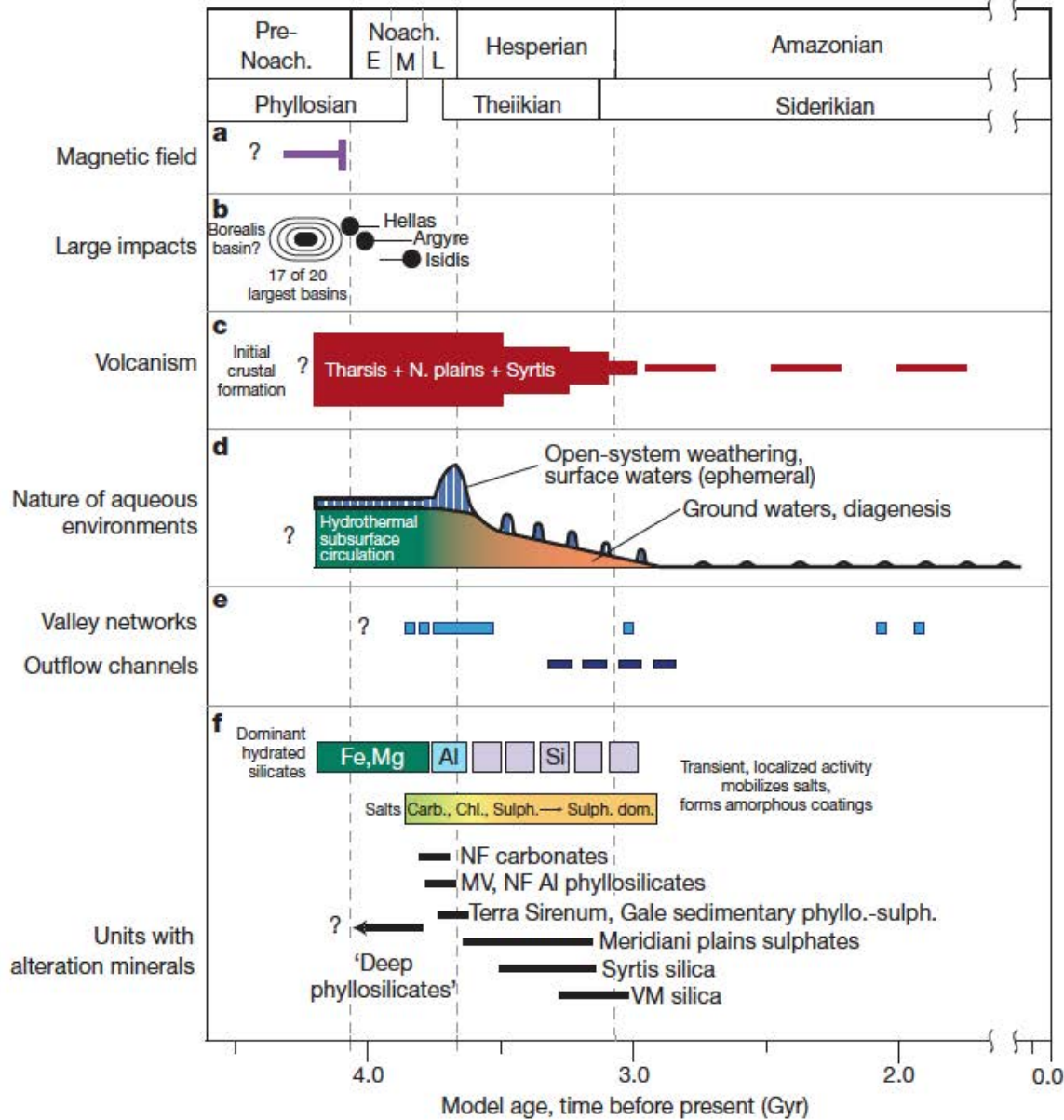
1976: Viking orbiters
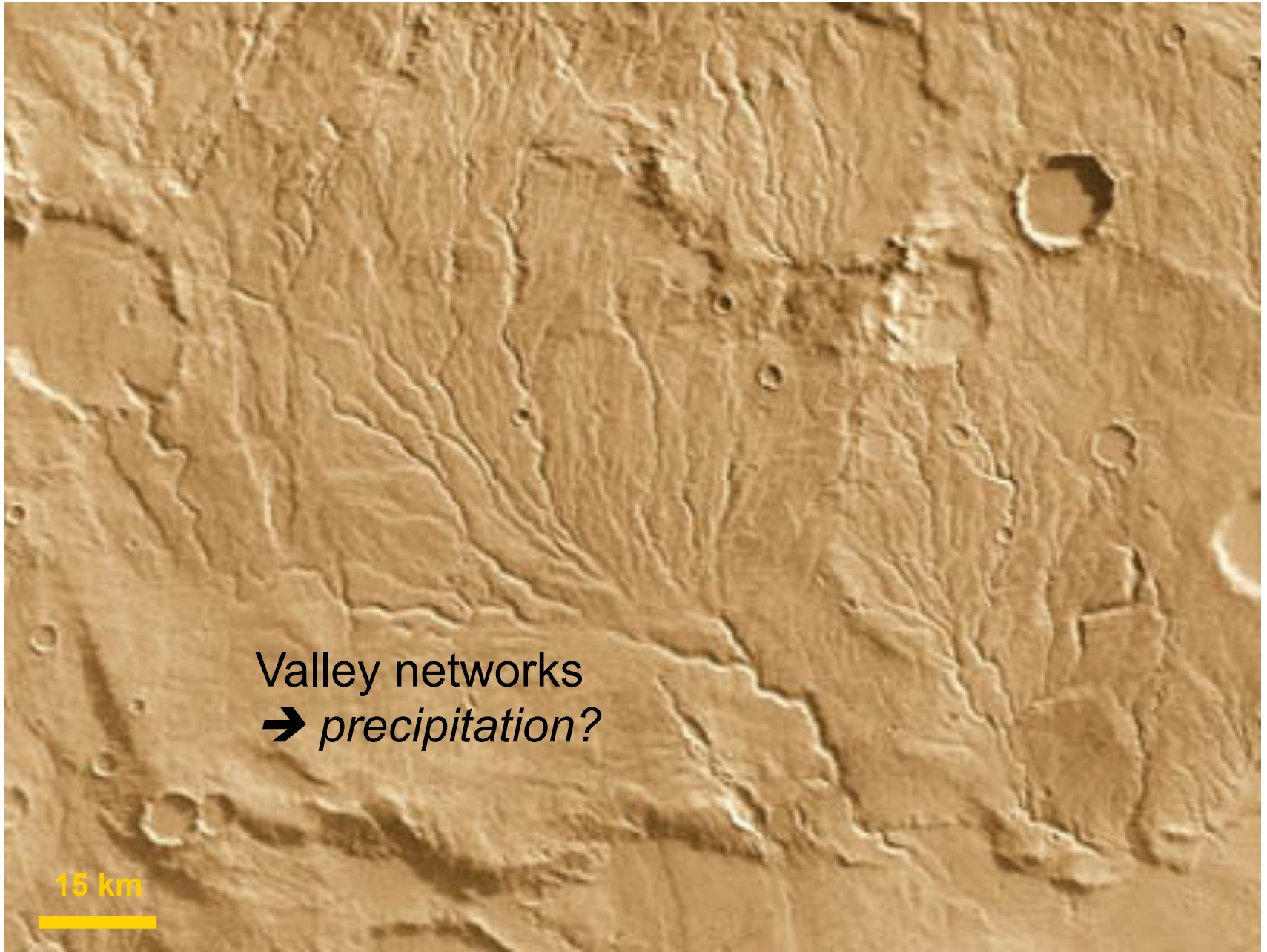

Valley networks
➔ *precipitation?*

15 km

Ehlmann et al. (2011a)

Figure 4 | Timeline of major processes in Mars history. a–c, Major geological processes influencing water availability, including the presence of a magnetic field[95] (a), impact cratering[96,97] (b) and volcanism[86,98] (c). **d,** Schematic depicting the changing nature of environments hosting liquid water, as implied by the geological evidence discussed herein. **e, f,** Evidence of liquid water: timing of valley network and outflow channel activity[15,16] ages of key minerals formed by aqueous alteration (e) and important regional units with alteration minerals (f). Relative timing is determined using relative crater densities and stratigraphic relationships. Absolute ages of period boundaries[5] have uncertainties of several hundred million years, inherent to extrapolation from cratering statistics[99]. NF, Nili Fossae; MV, Mawrth Vallis; VM, Valles Marineris; Carb., carbonates; Chl., chlorites; Sulph., sulphates.
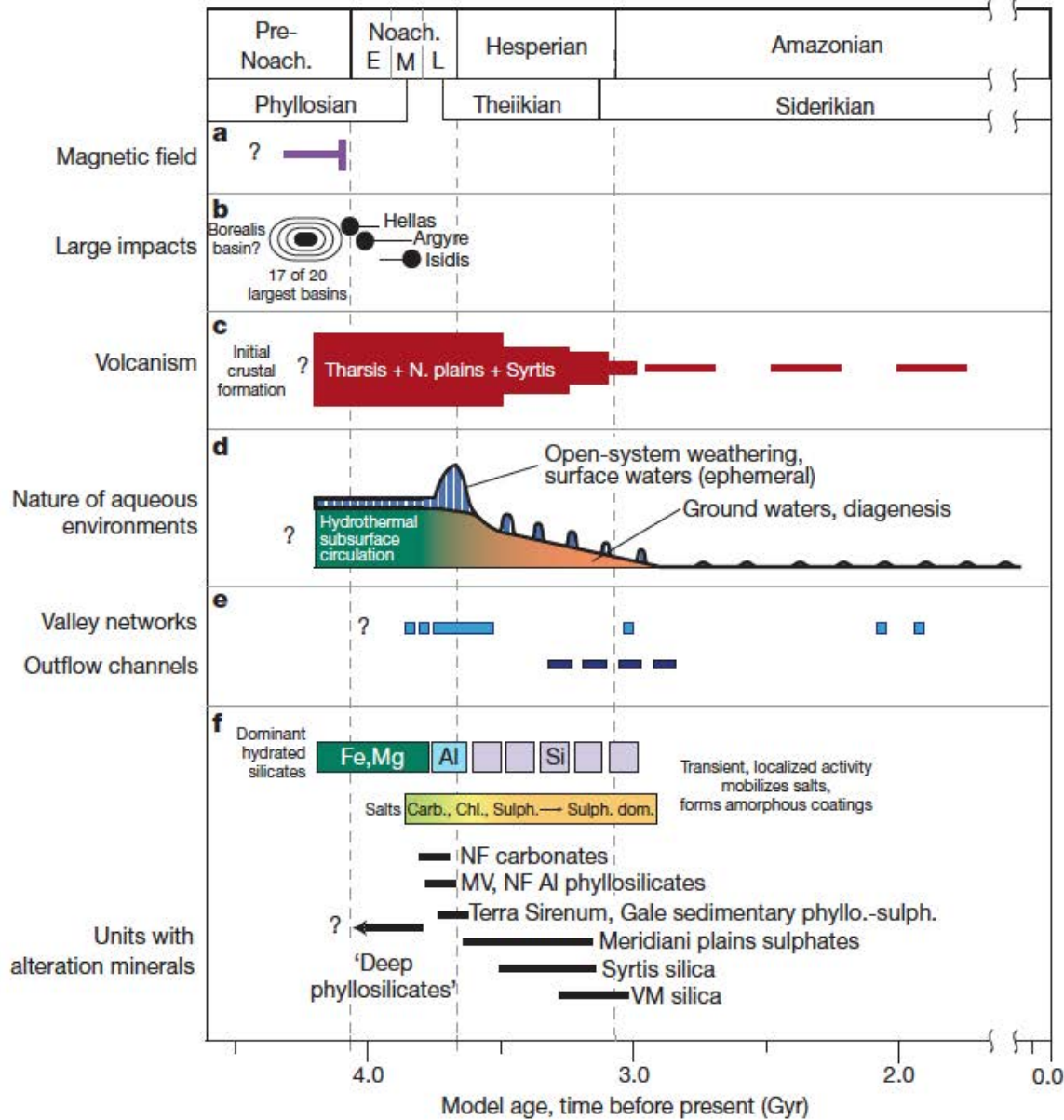
Caveat: alteration can also change bulk chemistry

1. ## Primary minerals
   - Olivine: $(Mg,Fe)_2SiO_4$
   - Pyroxene: $(Ca,Mg,Fe)SiO_3$
   - Plagioclase: $CaAl_2Si_2O_8 - NaAlSi_3O_8$

2. ## Oxides
   - Hematite: Fe_2O_3

3. ## Salts
   - Halite: $NaCl$
   - Gypsum: $CaSO_4 \cdot 2H_2O$
   - Calcite: $CaCO_3$

4. ## Secondary silicates (incl. phyllosilicates—e.g., clays)
   - Kaolinite: $Al_2Si_2O_5(OH)_4$
   - Nontronite: $Fe_2(Al,Si)_4O_{10}(OH)_2Na_{0.3} \cdot nH_2O$

Increasing water alteration

Mapping the water-related minerals

Figure 1. Distribution of major classes of aqueous minerals on Mars

● phyllosilicates ▢ chlorides ▲ sulfates ● carbonates
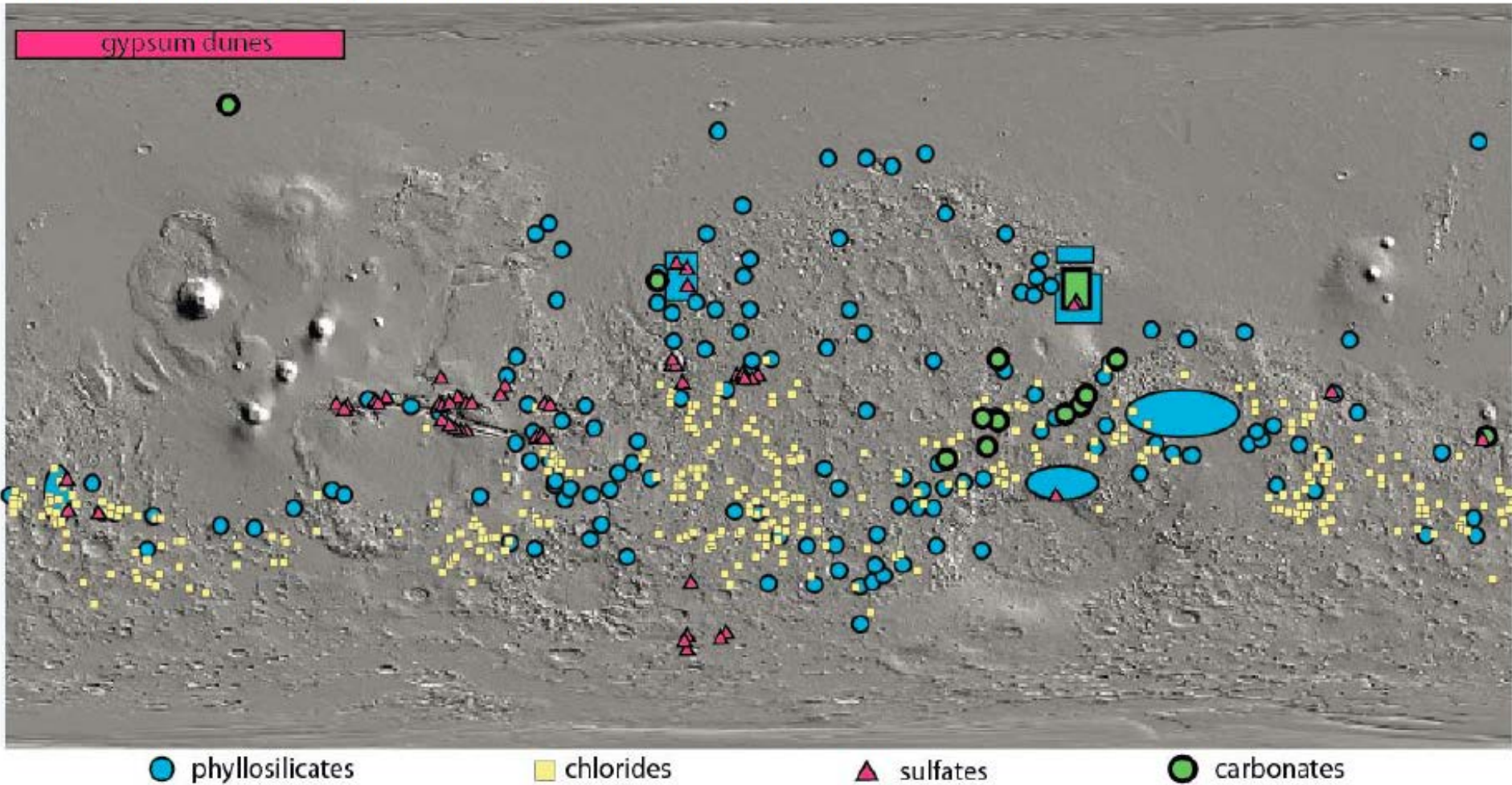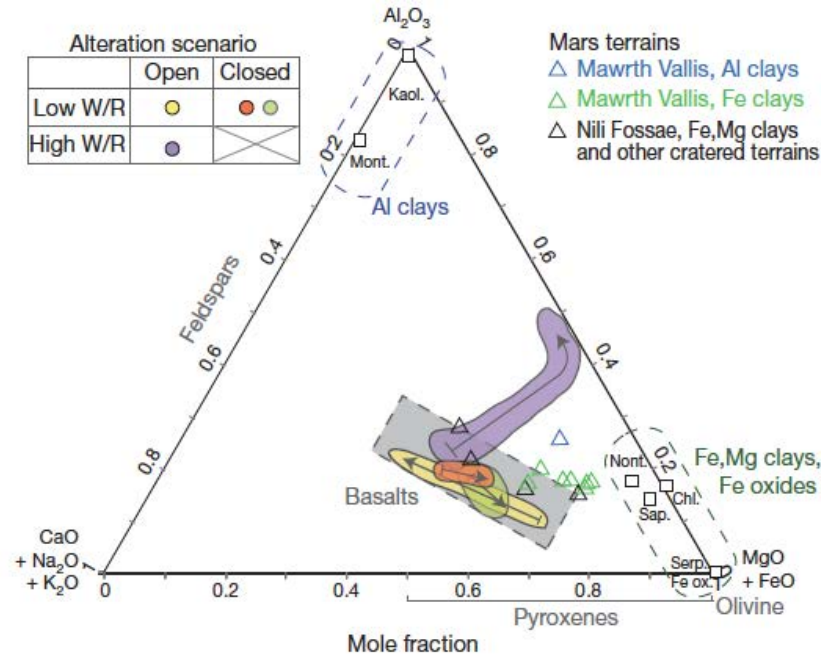
Ehlmann (2012)

Figure 2 | Chemical and mineralogical changes observed during aqueous alteration of basalt. Rocks of similar composition altered under different conditions show distinctive chemical changes characteristic of the alteration environment. Key parameters are the water-to-rock ratio (W/R) and whether the system is chemically open or closed to the atmosphere. Compositions of altered terrestrial basalts are plotted (after ref. 31) on a ternary diagram with major cations at the apices. The coloured regions encompass individual bulk-rock data points from the references (not shown), and arrows indicate the alteration trajectory. High-W/R, open-system weathering (purple[29]) leads to substantial chemical fractionation. Alkali and magnesium cations are removed, and primary minerals in rocks are replaced with aluminium clays and iron oxides. Cations liberated and transported during clay-forming reactions may subsequently form salts[32]. By contrast, low-W/R alteration results in little chemical fractionation and transport, although sample mineralogy changes. In open, low-W/R systems (yellow[31]), directionality of change is governed by olivine dissolution, and coatings of salts and amorphous products are generated by thin-film reactions before water evaporation. In closed, low-W/R systems (orange[27] and green[28]), primary minerals are replaced with Fe,Mg clay minerals and oxides and products such as silica and zeolites may precipitate in pore spaces[26]. Open triangles represent the chemical composition of clay-bearing units on Mars, calculated from estimates of dust-free modal mineralogy[74]. With the exception of aluminium-clay-bearing units in Mawrth Vallis, these lie on the mixing line between basalt and Fe,Mg clays expected for low-W/R, closed-system-type alteration. Chl., chlorite; Kaol, kaolinite; Mont., montmorillonite; Nont., nontronite; Sap., saponite; Serp., serpentine.

Ehlmann et al. (2011a)
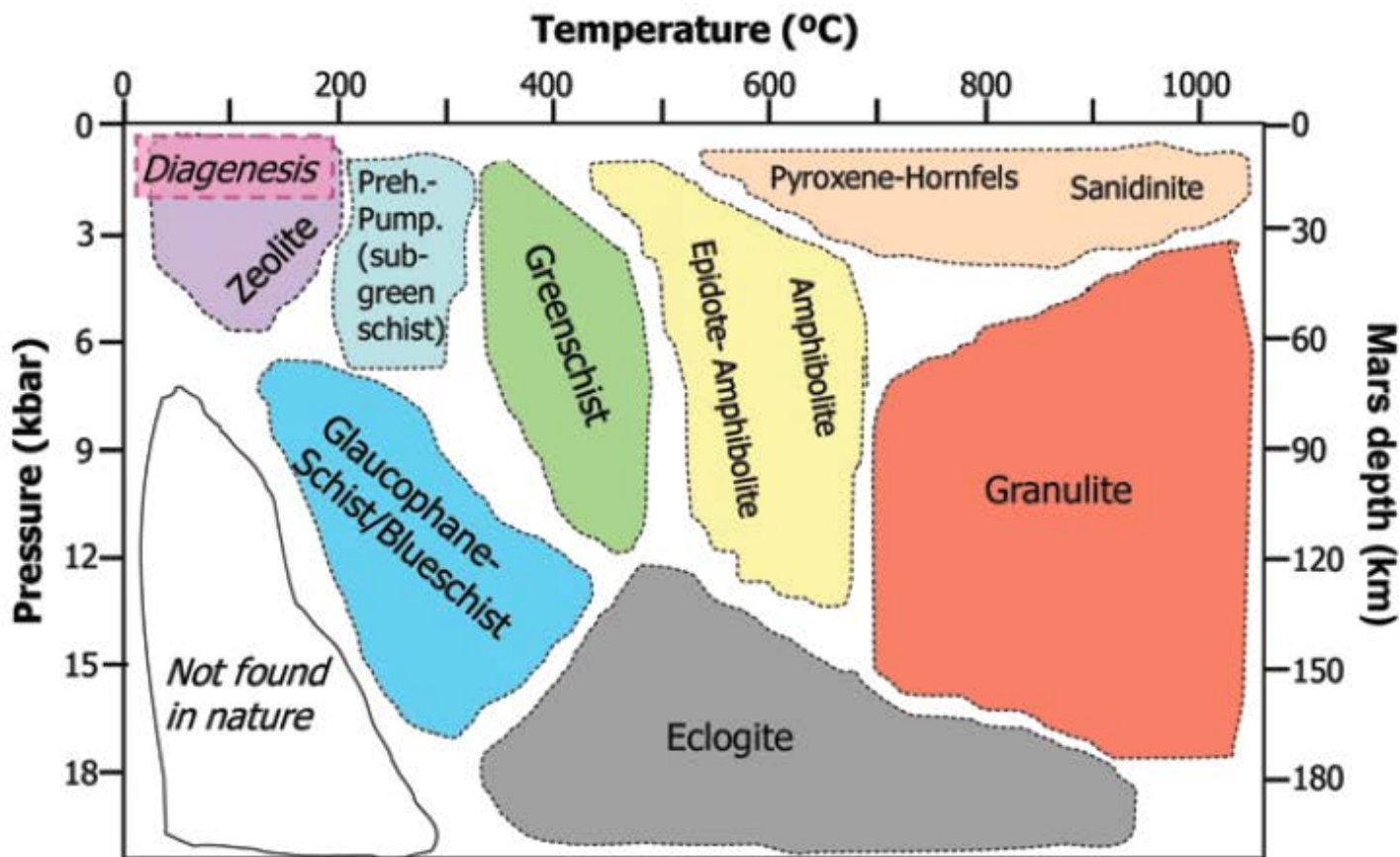
Metamorphic facies

Figure 1. Pressure-temperature metamorphic-facies diagram after Spear (1995). Greater depths than on Earth are required to achieve a given pressure because of Mars' lower gravity. Preh. = prehnite; Pump. = pumpellyite.

Ehlmann et al. (2011b)

Diagnostic minerals

Table 1. Common diagenetic mineral assemblages and diagnostic and common minerals for select metamorphic facies for a basaltic protolith (see Spear, 1995, chapter 11 for an overview, and specific references below).

P-T assemblage/facies	Diagnostic minerals and assemblages	Common minerals and assemblages	Specific references
Diagenesis	chlorite, illite or muscovite, and mixed-layer clays (chlorite/smectite, illite-smectite); celadonite+Fe,Mg-smectite		Cann (1979); Meunier (2005)
Zeolite	zeolite minerals	Heulandite + analcime + quartz, laumontite, stilbite, wairakite	Arkai *et al.* (2003); Coombs *et al.* (1959)
Sub-greenschist (prehnite-pumpellyite)	prehnite, pumpellyite	Prehnite + pumpellyite + chlorite, prehnite + chlorite + quartz, epidote + calcite + quartz + chlorite	Frey and Robinson (1999)
Greenschist	actinolite, cummingtonite	Chlorite + albite + actinolite (cummingtonite) + epidote + zoisite + quartz	Smulikowski *et al.* (2003); Philpotts and Ague (2009)
Amphibolite	hornblende	Hornblende + albite + epidote + chlorite, hornblende + Ca plagioclase (+ quartz + garnet)	Smulikowski *et al.* (2007); Philpotts and Ague (2009)
Blueschist	glaucophane, lawsonite	Glaucophane + lawsonite + garnet + quartz, glaucophane + lawsonite, glaucophane + lawsonite + jadeite	Smulikowski *et al.* (2007); Philpotts and Ague (2009)

Ehlmann et al. (2011b)
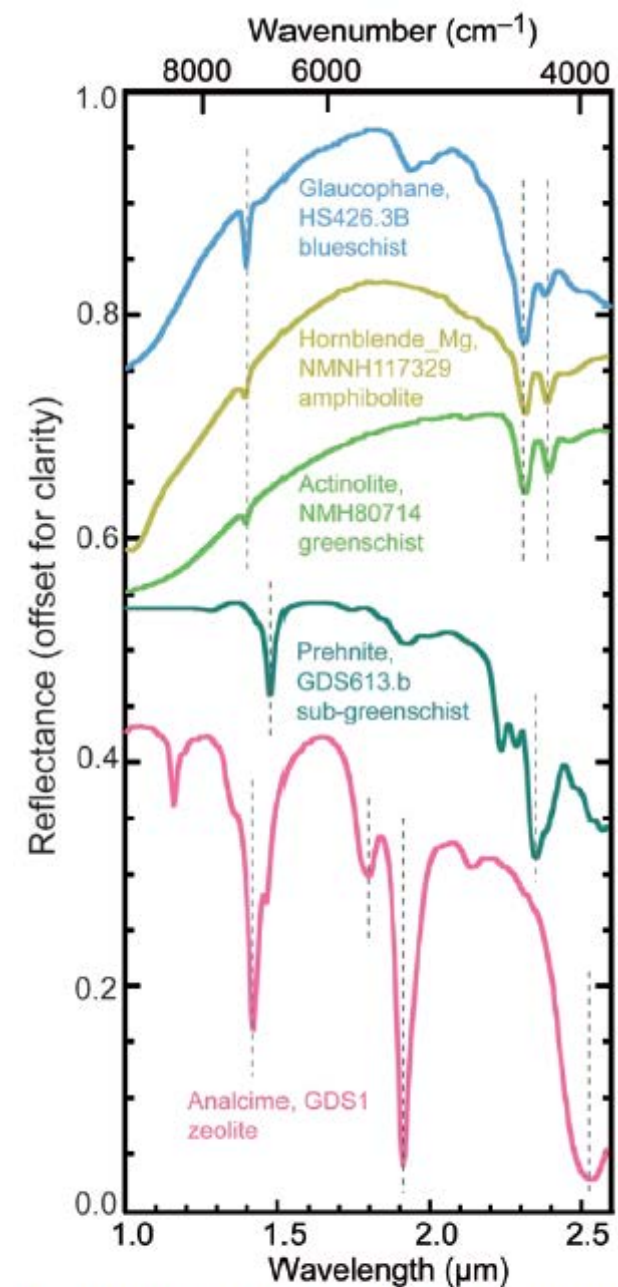
Spectroscopic methods

Figure 2. Sample VNIR spectra of diagnostic metamorphic minerals acquired in a laboratory (Clark *et al.*, 2007). Distinctive shapes and positions of absorption features permit these minerals to be identified on the surface of Mars using CRISM spectral data in the 1.0–2.6 µm wavelength range.

Ehlmann et al. (2011b)
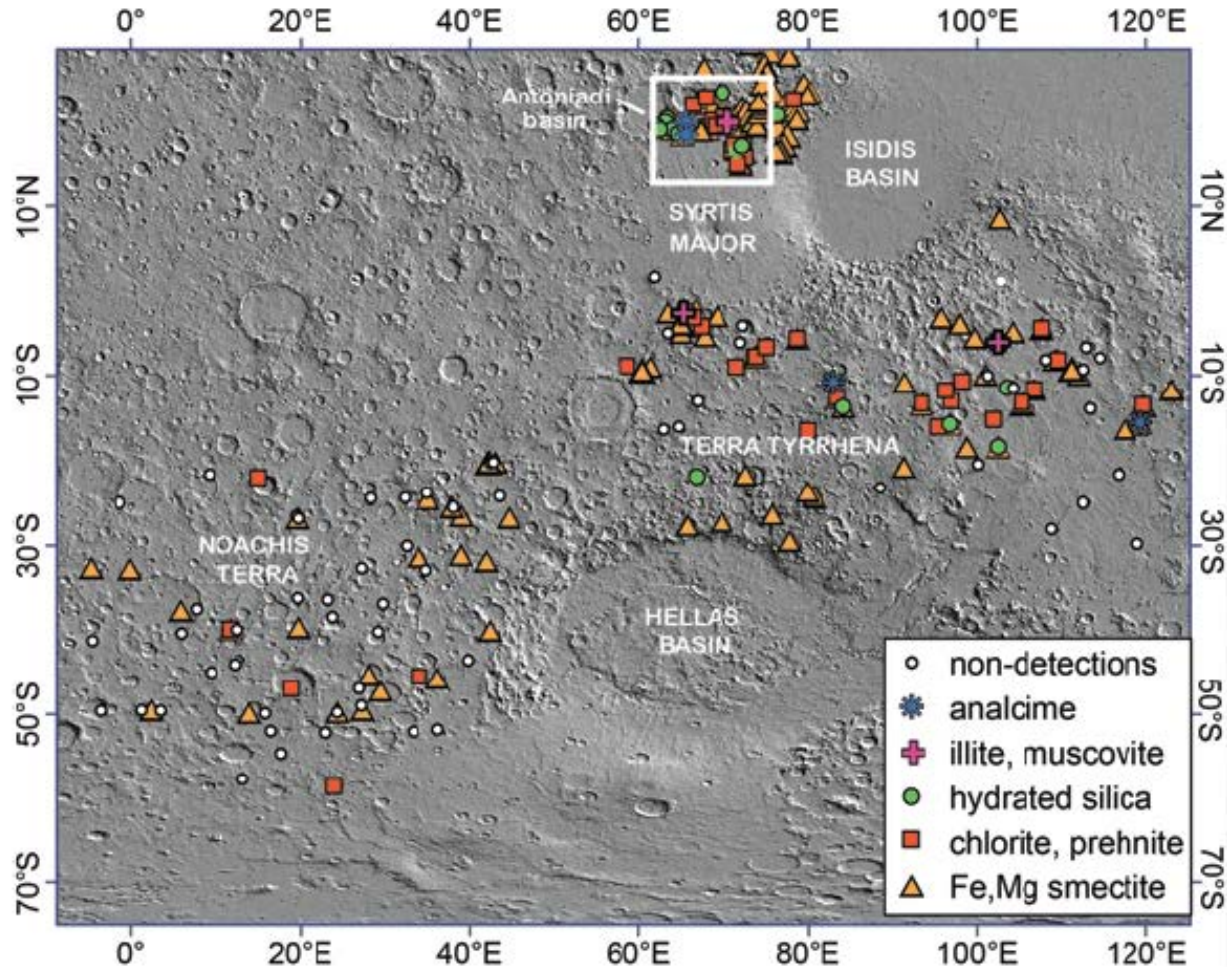
Diagnostic minerals

Figure 3. A Mars Orbiting Laser Altimeter (MOLA) hillshade map of the topography of Mars with mineral detections from a survey of CRISM targeted images overlain. Symbols represent minerals found within a CRISM image or group of images at a particular location (this spatial scale is too large to display the images). Fraeman *et al.* (2009) surveyed Noachis Terra and Terra Tyrrhena. Ehlmann *et al.* (2009) surveyed the area west of the Isidis basin. Fe,Mg-smectites are the most commonly detected alteration minerals, though localized instances of greater mineralogic diversity are observed. Examples for this review are taken from the area outlined by the white box.
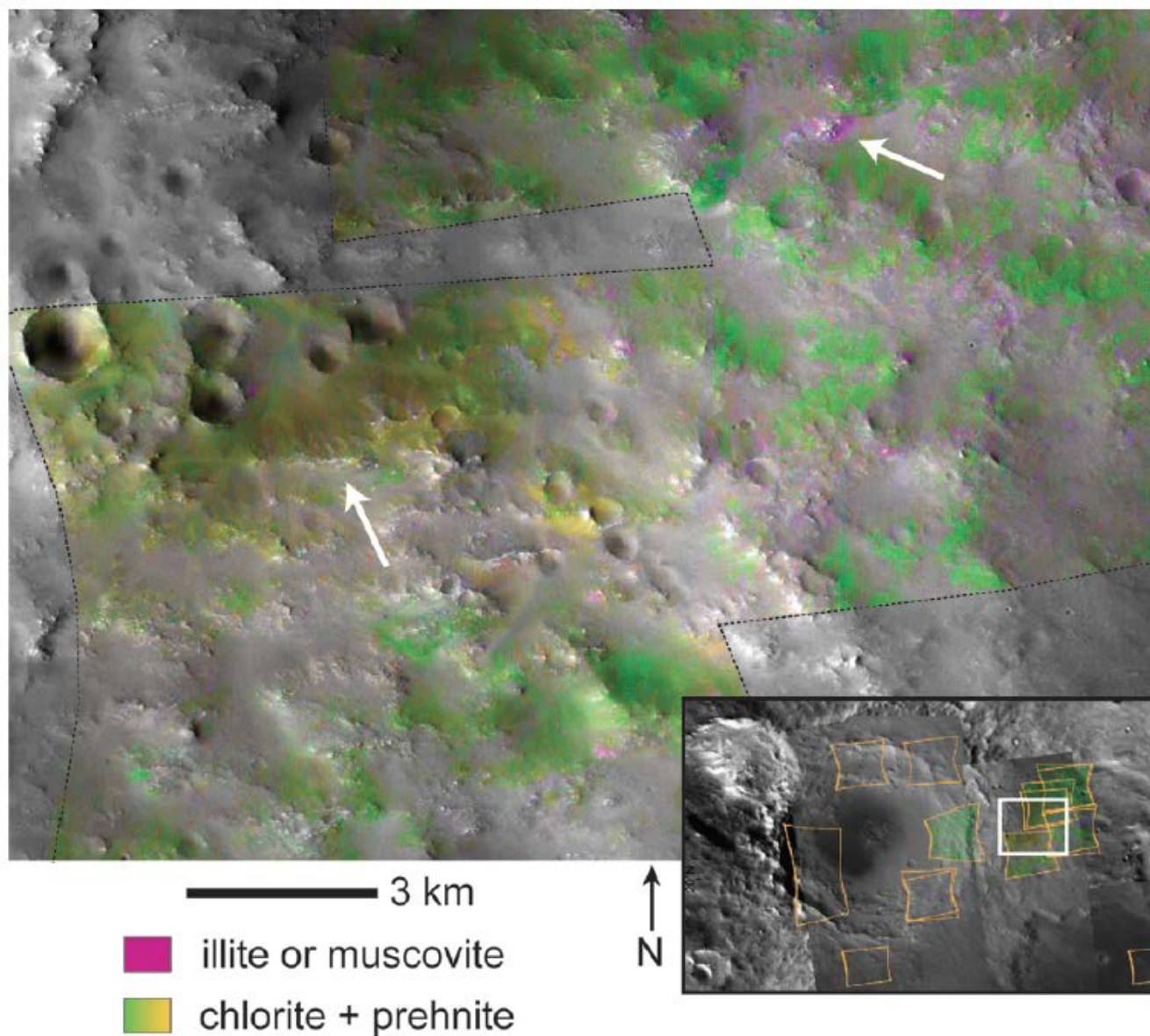
Ehlmann et al. (2011b)

Figure 7. Chlorite, prehnite, and illite (or muscovite; see text) are found within and around a 50 km impact crater in northern Syrtis Major (20°N, 69°E). The inset shows the context of the larger image which was made from a composite of CRISM images acquired on the eastern side of the crater within the zone of impact ejecta deposition. CRISM mineral maps were constructed by mapping absorption band depths at 2.35 μm (red), 2.3 μm (green), and 2.2 μm (blue), stretched so that pixels with spectra characteristic of illite or muscovite are magenta and chlorite or prehnite yellow to green (for yellow areas, the 2.35 μm absorption is sharper). These were overlain on a CTX image mosaic. The strongest mineral signatures coincide with rocky knobs and ridges (*e.g.* white arrows) and become weaker with distance from these knobs. Spectra from these CRISM images are shown in Figure 6 and were used to verify the color mapping of the mineralogy.

Ehlmann et al. (2011b)
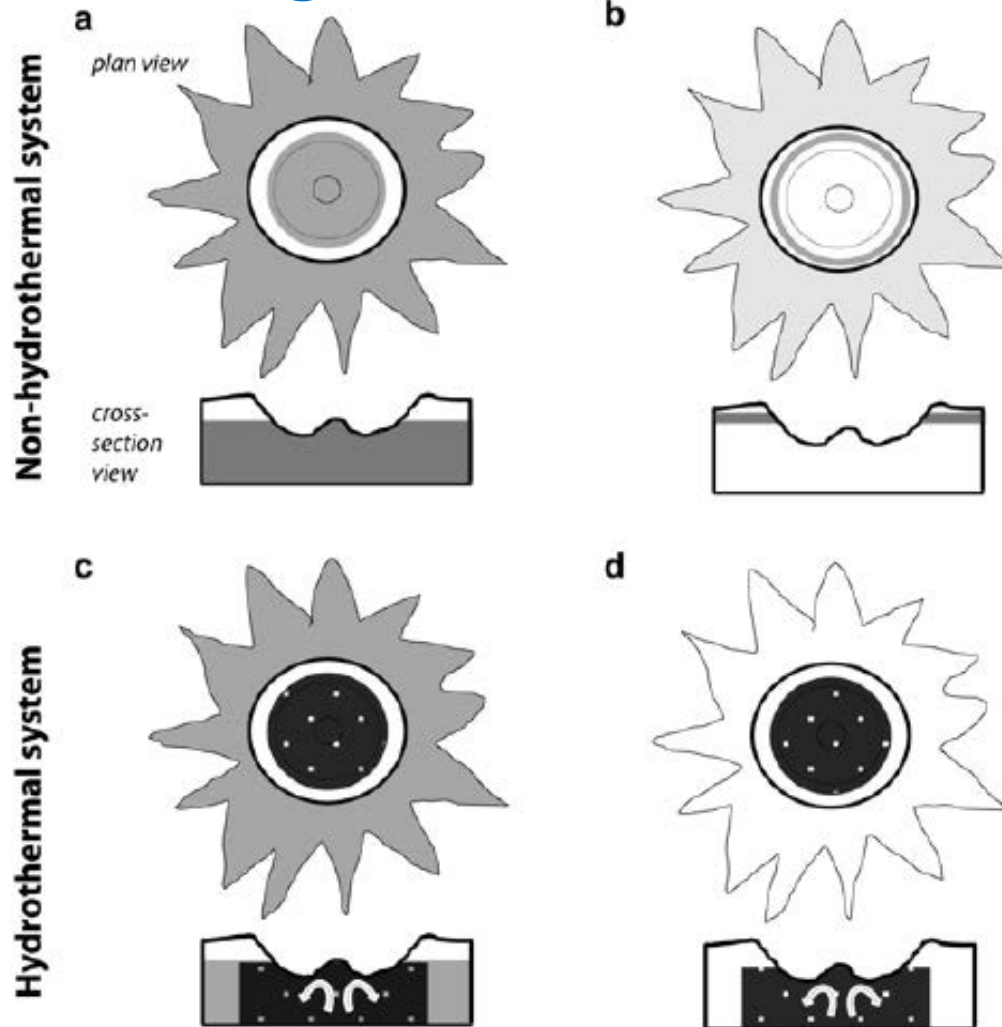
Diagnostic minerals

Figure 11. Schematic illustration of the mineral distribution around a crater expected as a result of the existence of a buried clay mineral-bearing stratum, a post-impact hydrothermal system, or both. Panels show the expected distribution for cratering (a) disturbing a thick, pre-existing clay layer, (b) disturbing a thin, pre-existing clay layer, (c) disturbing a thick, pre-existing clay layer with later post-impact hydrothermal activity, and (d) with later post-impact hydrothermal activity only. Minerals formed in a hydrothermal system (dark with white circles) would differ from pre-existing clays (gray). To date, only instances of clays with distribution like that in (a) and (b) have been found on Mars.

Ehlmann et al. (2011b)
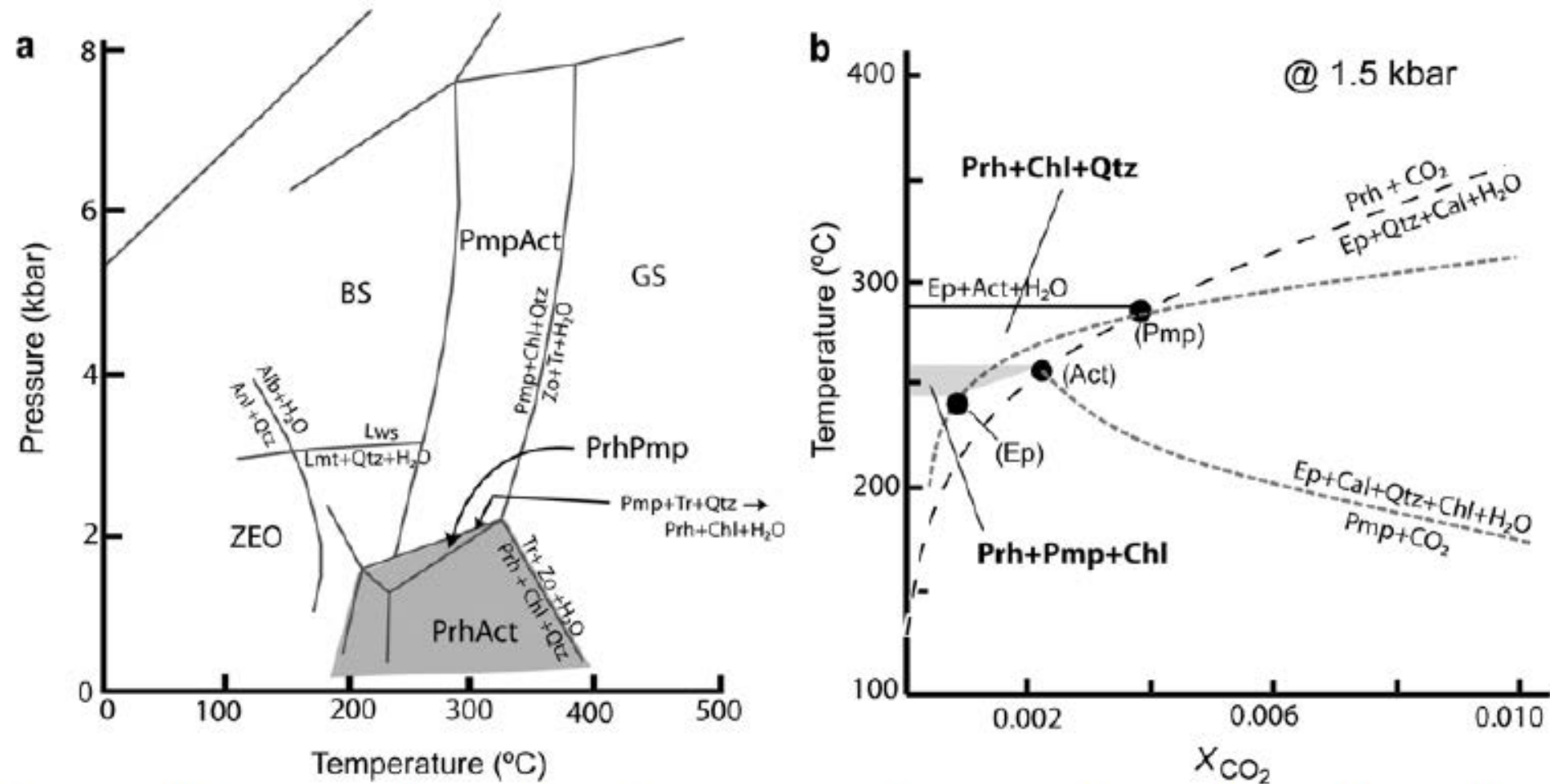
Diagnostic minerals

Figure 9. (a) Phase diagrams indicating prehnite stability as functions of temperature and pressure. Metamorphic facies (ZEO = zeolite, GS = greenschist, BS = blueschist) are indicated and selected reactions are shown (adapted from Schiffman and Day, 1999). (b) Temperature and mole fraction of CO_2 (adapted from Robinson and Bevins, 1999). Prh = prehnite, Pmp = pumpellyite, Chl = chlorite, Anl = analcime, Qtz = quartz, Alb = albite, Lws = lawsonite, Zo = zoisite, Tr = tremolite, Ep = epidote, Act = actinolite, Cal = calcite.

Ehlmann et al. (2011b)